Phase coexistence in polydisperse liquid mixtures: Beyond the van der Waals approximation

Yurij V. Kalyuzhnyi
Institute for Condensed Matter Physics, Svientsitskoho 1, 79011 Lviv, Ukraine and Center for Computational Materials Science and Institut für Theoretische Physik, TU Wien, Wiedner Hauptstrasse 8-10, A-1040 Wien, Austria

Gerhard Kahl[a)]
Center for Computational Materials Science and Institut für Theoretische Physik, TU Wien, Wiedner Hauptstrasse 8-10, A-1040 Wien, Austria

(Received 16 June 2003; accepted 18 July 2003)

The solution of the mean spherical approximation for a polydisperse fluid mixture of particles interacting via a set of (factorizable) hard-sphere Yukawa potentials allows one to represent those thermodynamic quantities that are relevant to determine phase coexistence (i.e., pressure and chemical potential) by a limited number of (generalized) moments. Being thus a member of ''truncatable free energy models,'' the equilibrium conditions reduce to a set of coupled and highly nonlinear equations; we have solved these relations, we have determined phase diagrams for polydisperse fluid mixtures (i.e., cloud and shadow curves as well as binodals), and have extracted the daughter distribution functions of the coexisting phases. © *2003 American Institute of Physics.* [DOI: 10.1063/1.1607952]

I. INTRODUCTION

Using microscopic liquid state theories,[1] it has become a standard task to determine phase coexistence in two- or even three-component fluid mixtures. However, when proceeding to *polydisperse* liquid mixtures (which can be viewed as a mixture with an infinite number of components), the situation is considerably more complex;[2] methods developed up to now to calculate phase diagrams for such systems have not yet reached the high level of sophistication as in concepts for systems with a *finite* number of components. This is the more deplorable since the (formally) infinite number of components promises a very intriguing phase coexistence behavior with possibly new phases and phase transitions. In addition, phenomena associated with the phase behavior of polydisperse systems, such as fractionation, are also of technological relevance.

Most of the concepts currently used to study polydisperse systems view such a system as a mixture with an infinite number of components, each of them characterized by a variable, for which one usually choses the particle size σ. The set of concentrations $\{x_i\}$ in a mixture with a finite number of components is replaced by a distribution function, $f(\sigma)$, which is positive and normalized, i.e., $\int_0^\infty d\sigma\, f(\sigma) = 1$. $f(\sigma_0)d\sigma$ is then the fraction of particles in the mixture whose size σ lies in an infinite interval of width $d\sigma$ around σ_0.

Standard liquid state theories have meanwhile been extended successfully to the polydisperse case [e.g., the Rogers–Young[3] or the optimized random phase approximation (ORPA)[4]]. Although these methods are able to deliver reliable information about the thermodynamic properties of such a system, up to now no satisfactory strategies have been developed to determine from these quantities the phase diagrams. The main obstacle lies in the coexistence conditions, in particular in the numerical complexity of the equilibrium condition for the chemical potentials which reads for two coexisting phases ''1'' and ''2,''

$$\mu_1(\sigma) = \mu_2(\sigma). \tag{1}$$

For a given mother distribution $f_0(\sigma)$, this equation has to be solved for each of the (infinitely many) σ's, or for a finite set of representative σ values $\{\sigma_i\}$. Its solution then leads to the unknown daughter distributions $f_1(\sigma)$ and $f_2(\sigma)$ of the coexisting phases. Recent attempts[5] to use the ORPA thermodynamic properties and to solve the coexistence conditions failed due to the complexity of Eq. (1).

At present one of the few ways out of this dilemma seems to resort to so-called truncatable free energy models; these are approximate schemes, where the thermodynamic properties of the system can be expressed by a limited number of (generalized) moments of the distribution functions $f_i(\sigma)$, $i=0,1,2$. Then, the solution of Eq. (1) can be mapped onto a coupled set of nonlinear equations for these moments, an access which is numerically more favorable. First steps in these directions were made with van der Waals models;[6,7] indeed results for complete phase diagrams (i.e., including cloud and shadow curves as well as binodals) could be presented. The question now arises if it is possible to go beyond a van der Waals model by including correlations while still maintaining the benefits of a truncatable free energy model.

In this contribution we show that this is indeed possible: We consider a polydisperse liquid mixture of hard-sphere Yukawa (HSY) fluids in the mean spherical approximation (MSA). This microscopic liquid state theory combines two attractive features which were very helpful to realize our

a)Electronic mail: gkahl@tph.tuwien.ac.at

goal: First, the MSA is known to give reasonably accurate results for the structure and thermodynamic properties of one- and two-component systems; second, the MSA can be solved for a HSY mixture with an arbitrary number of components[8,9] leading to closed (i.e., analytic) expressions for the thermodynamic properties. In particular, if one assumes *factorized* HSY interactions the numerical effort required for the MSA solution reduces drastically to the solution of one single nonlinear equation for the coupling constant Γ; this feature is preserved as we proceed to the polydisperse case.[10,11] Using this formalism we were indeed able to express pressure and chemical potential by a considerable (i.e., nine) but still finite set of (generalized) moments and coupling constant Γ. The coexistence conditions, by now a set of coupled nonlinear equations in the unknown moments of the two daughter distributions, have been solved and we were able to determine for a given mother distribution the complete phase diagram.

The paper is organized as follows: In Sec. II we present the theory (introducing our system, deriving expressions for the thermodynamic properties, justifying the distribution we have used, and discussing the numerical solution of the coexistence conditions). We then present results for a typical example and close the paper with concluding remarks.

II. THE THEORY

A. The system

We consider a polydisperse fluid mixture at a temperature $T[\beta=(k_BT)^{-1}]$ and a number density ρ, where particles of species x_1 and x_2 interact via HSY potential

$$\beta\Phi(r;x_1,x_2)=\begin{cases}\infty, & r\leqslant\sigma(x_1,x_2)\\ -\dfrac{K(x_1,x_2)}{r}\exp\{-z[r-\sigma(x_1,x_2)]\}, & \sigma(x_1,x_2)<r\leqslant\infty,\end{cases} \tag{2}$$

the hard-core potentials are characterized by a set of additive diameters, $\sigma(x_1,x_2)$, i.e.,

$$\sigma(x_1,x_2)=\tfrac{1}{2}[\sigma(x_1,x_1)+\sigma(x_2,x_2)] \tag{3}$$

with $\sigma(x,x)=\sigma$. In Eq. (2), z is the inverse screening length (which we assume to be constant, i.e., independent of particle size and potential amplitude) and the $K(x_1,x_2)$ are the contact values; here we use—for reasons outlined in the following—the following parametrization (which remains the only restrictive assumption of our model):

$$K(x_1,x_2)=\epsilon_0\sigma_0\beta Z(x_1)Z(x_2). \tag{4}$$

ϵ_0 is an energy parameter, σ_0 is the average sphere diameter (see the following), and the $Z(x_i)$ is the amplitude of the interatomic potential of a particle of species x_i; in an appropriate model it might also be interpreted as a charge. Thus for the model at hand the size (σ) and the amplitude (Z) of the particle completely define its species.

Size and amplitude of the particles are distributed according to a normalized distribution function $F(\sigma,Z)\geqslant 0$,

$$\int_0^\infty d\sigma\int_{-\infty}^{\infty}dZ\,F(\sigma,Z)=1. \tag{5}$$

Averages of quantities A taken over the distribution function $F(\sigma,Z)$ are denoted by $\langle A\rangle$; in particular, $\sigma_0=\langle\sigma\rangle$, $Z_0=\langle Z\rangle$.

B. Thermodynamic properties

For a general multicomponent HSY mixture the MSA can be solved in principle semianalytically;[9] this is done via a formalism which rapidly becomes involved as the number of components increases: systems of coupled nonlinear equations have to be solved. For *factorizable* HSY interactions [as introduced via Eq. (4)] this effort reduces substantially; even for an arbitrary (but finite) number of components, only one single nonlinear equation for the so-called coupling parameter Γ, the central quantity of this approach,[10] has to be solved.

As we proceed to the *polydisperse* case, we need a generalization of the Γ formalism; partly this has already been done in Ref. 11. In the following we briefly summarize the method, presenting those additional expressions which we require for the determination of the phase equilibrium and which have not been derived in literature so far.

The Γ formalism provides a closed expression for Helmholtz free energy F,[12]

$$\beta(F-F_{\mathrm{HS}})=\beta E_Y+\frac{\Gamma^2}{3\pi}\left(\Gamma+\frac{3}{2}z\right). \tag{6}$$

F_{HS} is the free energy of the HS system for which we have taken the expression due to Mansoori *et al.*,[13] generalized to the polydisperse case. E_Y and Γ are determined as follows:

$$\beta E_Y=K\left\{\rho\Gamma\int_0^\infty d\sigma\int_{-\infty}^{\infty}dZ\,F(\sigma,Z)Z\lambda(\sigma,Z)+\frac{\pi}{2\Delta}\frac{[\lambda^{(1)}]^2}{1+\xi^{(1)}}+\Delta_N(\lambda^{(0)}+\lambda^{(1)}E_N)\right\}. \tag{7}$$

$K=-\beta\epsilon_0\sigma_0$, $\Delta=1-\eta$ and η being the system packing fraction (see below).

Quantities used in this expression are

$$E_N=\frac{z}{2}+\Gamma-\frac{\pi}{2\Delta}\frac{\eta^{(1)}}{1+\xi^{(1)}}, \tag{8}$$

$$\Delta_N=\frac{2\pi\Delta_N[\lambda]}{z^2\Delta(1+\xi^{(1)})+2\pi\Delta_N[\eta]}, \tag{9}$$

$$\xi^{(n)}=\rho\int_0^\infty d\sigma\int_{-\infty}^{\infty}dZ\,F(\sigma,Z)\sigma^n\xi(\sigma), \tag{10}$$

$$\eta^{(n)}=\rho\int_0^\infty d\sigma\int_{-\infty}^{\infty}dZ\,F(\sigma,Z)\sigma^n\eta(\sigma), \tag{11}$$

$$\lambda^{(n)}=\rho\int_0^\infty d\sigma\int_{-\infty}^{\infty}dZ\,F(\sigma,Z)\sigma^n\lambda(\sigma,Z), \tag{12}$$

$$\zeta^{(n)}=\rho\int_0^\infty d\sigma\int_{-\infty}^{\infty}dZ\,F(\sigma,Z)\sigma^n,\quad \frac{\pi}{6}\zeta^{(3)}=\eta, \tag{13}$$

with

$$\xi(\sigma)=\frac{\pi}{2\Delta}\frac{\sigma^2\Phi_0(z\sigma)}{1+\Phi_0(z\sigma)\sigma\Gamma}, \tag{14}$$

$$\eta(\sigma)=\frac{z^2\sigma^3\Psi_1(z\sigma)}{1+\Phi_0(z\sigma)\sigma\Gamma}, \tag{15}$$

$$\lambda(\sigma,Z)=\frac{Z}{1+\Phi_0(z\sigma)\sigma\Gamma}, \tag{16}$$

$$\Delta_N[\chi]=\chi^{(1)}\left(\xi^{(0)}-\frac{z}{2}-\Gamma-\frac{\pi\zeta^{(2)}}{2\Delta}\right)-\chi^{(0)}(1+\xi^{(1)}), \tag{17}$$

where the $\chi^{(n)}$ stand either for the $\lambda^{(n)}$ or for the $\eta^{(n)}$.

Γ satisfies the following nonlinear algebraic equation:

$$\Gamma^2+z\Gamma=-\pi KD, \tag{18}$$

with

$$D=\rho\int_0^\infty d\sigma\int_{-\infty}^{\infty}dZ\,F(\sigma,Z)[X(\sigma)]^2 \tag{19}$$

and

$$X(\sigma)=\lambda\sigma-\frac{\lambda^{(1)}\xi(\sigma)}{1+\xi^{(1)}}-\Delta_N\left(\eta(\sigma)-\frac{\eta^{(1)}\xi(\sigma)}{1+\xi^{(1)}}\right). \tag{20}$$

Due to highly nonlinear character of Eq. (20) it has multiple solutions and the physical one, which reduces to $\Gamma=0$ in the high temperature limit, has to be chosen. In the present study we are using an iterative method of the solution similar to the one suggested earlier;[14] using the high temperature approximation $\Gamma=0$ as the initial input guarantees the proper (physical) solution of this equation.

In the above-noted expressions, the functions

$$\Phi_0(x)=\frac{1}{x}(1-e^{-x}) \tag{21}$$

and

$$\Psi_1(x)=\frac{1}{x^2}\left[-1+\left(1+\frac{x}{2}\right)\Phi_0(x)\right] \tag{22}$$

were introduced.

In addition, this Γ formalism provides closed expressions for the quantities that are required for the determination of the phase equilibrium: the pressure (P) and the chemical potential [$\mu(\sigma,Z)$] of a particle with size σ and amplitude Z. The expression for the pressure can be obtained by a straightforward generalization of the results for the discrete mixture,[11,12] i.e.,

$$\beta P=\beta P_{\mathrm{HS}}-\frac{\Gamma^2}{3\pi}\left(\Gamma+\frac{3}{2}z\right)+\frac{\pi K}{2\Delta^2}P_N\left(P_N+\frac{2z\Delta}{\pi}\Delta_N\right) \tag{23}$$

with

$$P_N=\frac{\lambda^{(1)}-\eta^{(1)}\Delta_N}{1+\xi^{(1)}}-\frac{z\Delta}{\pi}\Delta_N. \tag{24}$$

P_{HS} is the pressure of the HS reference system, again we use the semiempirical expression due to Mansoori *et al.*,[13] generalized to the polydisperse case

$$\beta P_{\mathrm{HS}}=\frac{1}{\Delta}\left\{\rho+\frac{\pi}{2\Delta}\zeta^{(1)}\zeta^{(2)}+\frac{\pi^2}{12\Delta^2}[\zeta^{(2)}]^3-\left(\frac{\pi}{6}\right)^3\frac{1}{\Delta^2}\zeta^{(3)}[\zeta^{(2)}]^3\right\}. \tag{25}$$

Expressions for the chemical potentials derived within the Γ formalism have not been presented so far in literature; they had to be developed for the present work. Using the standard relation between the free energy and chemical potential (generalized to the polydisperse case[2,15])

$$\mu(\sigma,Z)=\frac{1}{\rho}\frac{\delta\{F/V\}}{\delta\{F(\sigma,Z)\}}, \tag{26}$$

where $\delta/\delta\{F(\sigma,Z)\}$ denote functional differentiation with respect to the distribution $F(\sigma,Z)$, we find

$$\mu(\sigma,Z)=\mu_{\mathrm{id}}+\mu_{\mathrm{HS}}^{(\mathrm{ex})}(\sigma)+\mu_{\mathrm{Y}}^{(\mathrm{ex})}(\sigma,Z). \tag{27}$$

Here $\mu_Y^{(\mathrm{ex})}(\sigma,Z)$ is the Yukawa contribution to the chemical potential

$$\begin{aligned}\frac{\rho\beta}{K}\mu_Y^{(\mathrm{ex})}(\sigma,Z)&=\rho\lambda(\sigma,Z)\{Z\Gamma+\Delta_N(1+\sigma E_N)\}\\&+\frac{\delta\{\Delta_N\}}{\delta\{F(\sigma,Z)\}}(\lambda^{(0)}+\lambda^{(1)}E_N)+\frac{\pi\rho}{2\Delta}\frac{\sigma\lambda^{(1)}}{1+\xi^{(1)}}\\&\times\left\{(\lambda^{(1)}-\Delta_N\eta^{(1)})\left(\frac{\pi}{6\Delta}\sigma^2-\xi(\sigma)\right)\frac{\lambda^{(1)}-\Delta_N\eta^{(1)}}{1+\xi^{(1)}}\right.\\&\left.+2\lambda(\sigma,Z)-\Delta_N\eta(\sigma)\right\},\end{aligned} \tag{28}$$

where

$$\frac{\delta\{\Delta_N\}}{\delta\{F(\sigma,Z)\}}=\frac{2\pi}{z^2\Delta(1+\xi^{(1)})+2\pi\Delta_N[\eta]}\times\left[\frac{\delta\{\Delta_N[\lambda]\}}{\delta\{F(\sigma,Z)\}}-\Delta_N\left\{\frac{\delta\{\Delta_N[\eta]\}}{\delta\{F(\sigma,Z)\}}-\left(\frac{\sigma^2}{12}-\frac{\Delta}{2\pi}\xi(\sigma)\right)z^2\sigma\rho\right\}\right], \tag{29}$$

and

$$\frac{1}{\rho}\frac{\delta\{\Delta_N[\chi]\}}{\delta\{F(\sigma,Z)\}}=\left\{\sigma\left(\xi^{(0)}-\frac{z}{2}-\Gamma-\frac{\pi\zeta^{(2)}}{2\Delta}\right)-\xi^{(1)}-1\right\}\chi(\sigma,Z)+\left[\xi(\sigma)+\frac{\pi}{2\Delta}\sigma^2\left\{\sigma\left(\frac{1}{3}\xi^{(0)}-\frac{\pi}{6\Delta}\xi^{(2)}\right)-1\right\}\right]\chi^{(1)}-\left\{\xi(\sigma)+\frac{\pi}{6\Delta}\sigma^2\xi^{(1)}\right\}\sigma\chi^{(0)}; \tag{30}$$

again the χ's stand either for $\{\lambda^{(0)},\lambda^{(1)},\lambda(\sigma,Z)\}$ from Eqs. (12) and (16) or $\{\eta^{(0)},\eta^{(1)},\eta(\sigma)\}$ from Eqs. (11) and (15). Expression (28) for $\mu_Y^{(\mathrm{ex})}(\sigma,Z)$ was derived using the stationarity property of the MSA Helmholtz free energy[12]

$$\frac{\partial F}{\partial\Gamma}=0. \tag{31}$$

Consistent with our choice of the expressions for F_{HS} and P_{HS}, the excess chemical potential of the reference hard-sphere system $\mu_{\mathrm{HS}}^{(\mathrm{ex})}$ in Eq. (27) is represented by the polydisperse version of the Mansoori *et al.*[13] expression, i.e.,

$$\beta\mu_{\mathrm{HS}}^{(\mathrm{ex})}(\sigma)=\left\{\left[\sigma\frac{\zeta^{(2)}}{\zeta^{(3)}}\right]^2\left[3-2\sigma\frac{\zeta^{(2)}}{\zeta^{(3)}}\right]-1\right\}\ln\Delta+\frac{\pi}{2\Delta}\sigma\left[\frac{1}{3}\sigma^2\left\{\rho-\frac{[\zeta^{(2)}]^3}{[\zeta^{(3)}]^2}\frac{1+\Delta}{\Delta}+\frac{\pi}{\Delta}\zeta^{(2)}\left(\frac{1}{2}\zeta^{(1)}+\frac{1}{3}\frac{[\zeta^{(2)}]^2}{\zeta^{(3)}\Delta}\right)\right\}+\zeta^{(2)}\left(1+\frac{\zeta^{(2)}\sigma}{\zeta^{(3)}\Delta}\right)+\sigma\zeta^{(1)}\right]. \tag{32}$$

C. The distributions

A distribution $F(\sigma,Z)$ as introduced earlier for the size and the amplitude of the particles allows an independent variation of these two system parameters. Since the main goal of this work is the presentation of the formalism, we have used a simplified expression (which can also be motivated from the physical point of view), namely[3]

$$F(\sigma,Z)=f(\sigma)\delta\left(Z-Z_0\frac{\sigma^2}{\langle\sigma^2\rangle}\right), \tag{33}$$

where $\langle\sigma^2\rangle=\int_0^\infty\sigma^2 f(\sigma)d\sigma$ and $\delta(...)$ is the Dirac delta function.

This choice is physically sound, since it states that the amplitude is proportional to the surface of the particles; from a more practical point of view it reduces double integrals over *σ and Z* (listed earlier) to integrals over *σ only*. Thus the complexity of the coexistence conditions is brought down to a level which is still tractable in practical applications.

For $f(\sigma)$ we have chosen the beta distribution, given by

$$f(\sigma)=B^{-1}(\alpha,\beta)\left(\frac{\sigma}{\sigma_m}\right)^{\alpha-1}\left(1-\frac{\sigma}{\sigma_m}\right)^{\beta-1}\Theta(\sigma_m-\sigma)\Theta(\sigma), \tag{34}$$

where

$$\Theta(x)=\begin{cases}1, & x\geqslant 0\\ 0, & x<0.\end{cases}$$

$f(\sigma)$ is thus different from zero only for $\sigma\in[0,\sigma_m]$. $B(\alpha,\beta)$ is the beta function[16] and α and β are related to the first ($\sigma_0=\langle\sigma\rangle$) and the second ($\langle\sigma^2\rangle$) moments of $f(\sigma)$ by

$$\alpha=\frac{\sigma_m-\sigma_0(1+D_\sigma)}{\sigma_m D_\sigma}, \tag{35}$$

$$\beta=\left(\frac{\sigma_m-\sigma_0}{\sigma_0}\right)\alpha \tag{36}$$

with $D_\sigma=\langle\sigma^2\rangle/\sigma_0^2-1$; D_σ has the same meaning as in Ref. 11 and corresponds to $(1/\alpha)$ in Ref. 7.

This particular choice for the distribution function was motivated by the fact that—in contrast to other distribution functions frequently used in this field, such as the Schulz distribution[17]—the beta distribution has a limited carrier, i.e., this function is exactly zero beyond σ_m. Use of the Schulz distribution (with $\sigma\in[0,\infty]$) on the other hand, allows—even though with an extremely small probability—the occurrence of huge particles, with—as a consequence of Eq. (33)—an extremely strong Yukawa interaction; from unpublished results we find evidence, that in particular these strong attractions make us pass the limits of applicability of the MSA, leading to unphysical results for the phase diagram. Problems with distributions with an infinite carrier were also reported in Refs. 18 and 19.

D. Phase equilibrium

The way in which the equilibrium conditions (1) are mapped in a truncatable free energy model onto a system of coupled equations for the unknown generalized moments closely follows the work of Bellier-Castella *et al.*;[7] we therefore briefly summarize this route here.

We shall restrict ourselves in this contribution to two-phase coexistence. We denote the distribution function of the mother phase as $f_0(\sigma)$ and its number density ρ_0; we want to determine the distribution functions of the two daughter phases $[f_i(\sigma)]$, and their number densities ρ_i, $i=1,2$. As a consequence of the conservation of the total number of particles of each species (characterized by a diameter σ), the following relation holds:

$$\rho_2 f_2(\sigma)=\frac{\rho_1-\rho_2}{\rho_1-\rho_0}\rho_0 f_0(\sigma)+\frac{\rho_0-\rho_2}{\rho_0-\rho_1}\rho_1 f_1(\sigma). \tag{37}$$

At a given temperature T, we are thus left with two unknown densities, ρ_1 and ρ_2, and one unknown daughter distribution function, eliminating the other one via Eq. (37). Hence we have to derive three relations. As shown in Ref. 7, the first relation is given by

$$f_1(\sigma)=f_2(\sigma)\frac{\rho_2}{\rho_1}\exp[\beta\Delta\mu^{(\mathrm{ex})}] \tag{38}$$

with

$$\Delta\mu^{(\mathrm{ex})}=\mu^{(\mathrm{ex})}(\sigma,Z,T;\rho_2;[f_2])-\mu^{(\mathrm{ex})}(\sigma,Z,T;\rho_1;[f_1]) \tag{39}$$

and $\mu^{(\mathrm{ex})}=\mu^{(\mathrm{ex})}_{\mathrm{HS}}(\sigma)+\mu^{(\mathrm{ex})}_{\mathrm{Y}}(\sigma,Z)$ with hard-sphere and Yukawa contributions given by Eqs. (32) and (28). Here the square brackets indicate functional dependencies. $f_2(\sigma)$ or $f_1(\sigma)$ can be eliminated from Eq. (38) via Eq. (37) to give either

$$f_1(\sigma)=f_0(\sigma)Q_1(\sigma,T;\rho_0,\rho_1,\rho_2;[f_1]), \tag{40}$$

where

$$\rho_1 Q_1(\sigma,T;\rho_0,\rho_1,\rho_2;[f_1])=\frac{\rho_0(\rho_2-\rho_1)\exp(\beta\Delta\mu_{\mathrm{ex}})}{(\rho_0-\rho_1)-(\rho_0-\rho_2)\exp(\beta\Delta\mu_{\mathrm{ex}})}, \tag{41}$$

or

$$f_2(\sigma)=f_0(\sigma)Q_2(\sigma,T;\rho_0,\rho_1,\rho_2;[f_2]), \tag{42}$$

where

$$\rho_2 Q_2(\sigma,T;\rho_0,\rho_1,\rho_2;[f_2])=\frac{1}{(\rho_0-\rho_1)-(\rho_0-\rho_2)\exp(\beta\Delta\mu_{\mathrm{ex}})}. \tag{43}$$

The second relation is the normalization condition, i.e.,

$$1=\int_0^\infty d\sigma\, f_i(\sigma), \quad i=1,2, \tag{44}$$

and the third one is the equality of the pressure in both phases,

$$P(T;\rho_1;[f_1])=P(T;\rho_2;[f_2]). \tag{45}$$

Formally the set of relations (38), (44), and (45) form a closed set of equations for the unknowns ρ_1, ρ_2, and $f_1(\sigma)$: they have to be solved for every σ value or for a set of representative σ values. This task seems at present out of reach from the numerical point of view and we choose a different route which is much more attractive and more easily accessible: a closer analysis of Eqs. (6), (23), and (27) reveals that the thermodynamic properties of the model at hand are defined by the temperature T, the density ρ of the system, the set of nine generalized moments $\xi^{(n)}$, $\eta^{(n)}$, $\lambda^{(n)}$ $(n=0,1)$, $\zeta^{(n)}$ $(n=1,2,3)$, and the coupling parameter Γ. This feature allows us to map the set of relations (38), (44), and (45) onto a closed set of twenty-two algebraic equations for the eighteen generalized moments, the two densities ρ_1 and ρ_2, and the two Γ parameters of the two coexisting phases (Γ_1 and Γ_2). Using relations (10)–(13), along with (40) and (42) we have

$$\xi_i^{(n)}=\rho_i\int_0^\infty d\sigma\,\sigma^n\xi_i(\sigma)f_0(\sigma)\times Q_i(\sigma,T;\rho_0,\rho_1,\rho_2;[\Gamma_1;\{\xi\eta\lambda\zeta\}_1],[\Gamma_2;\{\xi\eta\lambda\zeta\}_2]), \quad i=1,2, \quad n=0,1, \tag{46}$$

$$\eta_i^{(n)}=\rho_i\int_0^\infty d\sigma\,\sigma^n\eta_i(\sigma)f_0(\sigma)\times Q_i(\sigma,T;\rho_0,\rho_1,\rho_2;[\Gamma_1;\{\xi\eta\lambda\zeta\}_1],[\Gamma_2;\{\xi\eta\lambda\zeta\}_2]), \quad i=1,2, \quad n=0,1, \tag{47}$$

$$\lambda_i^{(n)}=\rho_i\int_0^\infty d\sigma\,\sigma^n\lambda_i(\sigma)f_0(\sigma)\times Q_i(\sigma,T;\rho_0,\rho_1,\rho_2;[\Gamma_1;\{\xi\eta\lambda\zeta\}_1],[\Gamma_2;\{\xi\eta\lambda\zeta\}_2]), \quad i=1,2, \quad n=0,1, \tag{48}$$

$$\zeta_i^{(n)}=\rho_i\int_0^\infty d\sigma\,\sigma^n f_0(\sigma)\times Q_i(\sigma,T;\rho_0,\rho_1,\rho_2;[\Gamma_1;\{\xi\eta\lambda\zeta\}_1],[\Gamma_2;\{\xi\eta\lambda\zeta\}_2]), \quad i=1,2, \quad n=1,2,3, \tag{49}$$

which represent eighteen relations. Note in the above-given notation that the dependence on the set of parameters $[\Gamma_i;\{\xi\eta\lambda\zeta\}_i]$ is equivalent to the functional dependence of the above functions on the $[f_i]$, $i=1,2$. Here and in the following the $\{\xi\eta\lambda\zeta\}_i$ denote the set of the moments $\xi_i^{(n)}$, $\eta_i^{(n)}$, $\lambda_i^{(n)}$, $\zeta_i^{(n)}$, $i=1,2$ and n values as indicated in the above equations.

The remaining four equations are found from the normalization condition (44),

$$1=\int_0^\infty d\sigma\, f_0(\sigma)\times Q_i(\sigma,T;\rho_0,\rho_1,\rho_2;[\Gamma_1;\{\xi\eta\lambda\zeta\}_1],[\Gamma_2;\{\xi\eta\lambda\zeta\}_2]), \quad i=1,2, \tag{50}$$

by the equality of the pressure in both phases (45),

$$P(T;\rho_1;[\Gamma_1;\{\xi\eta\lambda\zeta\}_1])=P(T;\rho_2;[\Gamma_2;\{\xi\eta\lambda\zeta\}_2]), \tag{51}$$

and by Eq. (18), written down for the scaling parameters Γ in each of the two phases

$$\Gamma_i^2+z\Gamma_i=-\pi K D_i, \quad i=1,2. \tag{52}$$

In Eqs. (46)–(52) the quantities with the lower index equal 1 (or 2) represent the corresponding values for the first (or second) phase.

Solution of this set of equations leads to the binodal curves and via Eqs. (40)–(43) to the distribution functions $[f_i(\sigma)]$ of the coexisting two daughter phases for the given value of the mother phase density ρ_0 and mother distribution function $f_0(\sigma)$. In general in polydisperse systems binodal

curves do not meet at the critical point; they are terminated at temperatures for which the density of either phase becomes equal to the density of the mother phase. The set of these terminal points for different ρ_0 defines the so-called cloud and shadow curves. The cloud curve represents the terminal points of the phase with the density equal to ρ_0 and the shadow curve consists of the points in equilibrium with the corresponding cloud-curve points. Thus the cloud and shadow curves are of particular interest, since they represent an envelope for the binodals.

By definition the cloud phase coexists with an infinitesimal amount of the shadow phase. Thus the cloud and shadow curves can be obtained as a special solution of the general phase coexistence problem where the properties of one phase are equal to those of the mother phase. Assuming, e.g., the second phase to be the cloud phase, i.e., $\rho_2=\rho_0$, and following the above-presented scheme, the twenty-two equations of the *full* coexistence problem reduce to a set of twelve equations: it is represented by Eqs. (46)–(52) for the special choice of $i=1$, $\rho_2=\rho_0$, $\Gamma_2=\Gamma_0$, and $\{\xi\eta\lambda\zeta\}_2=\{\xi\eta\lambda\zeta\}_0$; the unknowns are $\xi_1^{(n)}$, $\eta_1^{(n)}$, $\lambda_1^{(n)}$, $\zeta_1^{(n)}$ [with *n*-values as indicated in Eqs. (46)–(49)], Γ_1, ρ_1, and ρ_0.

To obtain a solution for the *general* coexistence problem from the above-noted set of equations a numerical scheme has been utilized, which combines an iterative loop for the solution of the equation for Γ (52) and a Newton–Raphson method for the remaining equations. Following a suggestion made earlier[14] we rewrite Eq. (52) in a form more appropriate for numerical iterations,

$$\Gamma_i=-\frac{\pi K D_i}{z+\Gamma_i}, \quad i=1,2. \tag{53}$$

Starting from some suitable set of starting values (see the following), results of the previous iteration cycle for Γ_i and the moments (obtained from the Newton–Raphson algorithm) are used in the right-hand side of Eq. (53) as an input for the next iteration cycle. New values of Γ_i, which follow from Eq. (53), are then utilized to solve the set of equations (46)–(51) for the moments via the Newton–Raphson algorithm. We start at a relatively high temperature and a low degree of the polydispersity: as the initial input we have used the high temperature approximation for the Γ_i, i.e., $\Gamma_i=0$, the coexistence densities of the one component (i.e., monodisperse) case, $\rho_{1;\mathrm{oc}}$ and $\rho_{2;\mathrm{oc}}$, for the densities ρ_i, and the mother phase distribution as a first guess for the daughter phase distributions, i.e., $f_1(\sigma)=f_2(\sigma)=f_0(\sigma)$. Solution of the set of equations (46)–(52) is then obtained by gradually lowering the temperature and increasing polydispersity.

III. RESULTS

We now present results for the phase diagram of a specific polydisperse system. It is characterized by a mother distribution function $F_0(\sigma,Z)$ for which we have chosen the form (33), i.e., the amplitude is proportional to the surface; thus $F_0(\sigma,Z)=f_0(\sigma)\,\delta(Z-Z_0(\sigma^2/\langle\sigma^2\rangle))$. $f_0(\sigma)$ is a beta distribution (34) with $D_\sigma=0.02$ and $\sigma_m=2\sigma_0$. The screening length of the Yukawa potential (2) was chosen to be $z\sigma_0=1.8$. In what follows the temperature T and density ρ of the system will be represented by the dimensionless quantities $T^*=kT/(\epsilon_0 Z_0^2)$ and $\rho^*=\rho\sigma_0^3$, respectively.

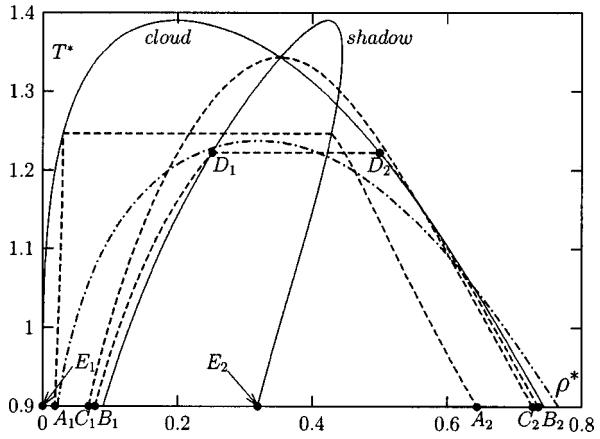

FIG. 1. Phase diagram (T^* vs ρ^*) of the polydisperse HSY mixture specified in the text. Five pairs of points (labeled A_i to E_i, $i=1,2$) are marked on the curves; they are specified in Table I. Cloud and shadow curves are represented by the solid lines (as labeled), binodal curves for the polydisperse HSY mixture by the broken lines connecting the points, which mark the density of the corresponding mother phase, i.e., $\rho_0^*=0.03$ (A_1---A_2), $\rho_0^*=\rho_c^*=0.3527$ (C_1---C_2), $\rho_0=0.5$ (B_1---B_2); the dot–dashed line denotes the binodal curve for the monodisperse HSY system.

In Fig. 1 we show the phase diagram of the system in the (T^*,ρ^*) plane: it contains the cloud and the shadow curve, the critical binodal (see the following) and binodals for two selected ρ_0^* values ($\rho_0^*=0.03$ and $\rho_0^*=0.5$). For the critical point we find $T_{\mathrm{cr}}^*=1.343$ and $\rho_{\mathrm{cr}}^*=0.3527$. ρ_{cr} was determined in an iterative scheme from a sequence of $\{\rho_{[i]}\}$ which—by definition—must tend toward ρ_{cr}: we choose a density $\rho_{[0]}$ and a temperature T and calculate—by increasing the temperature—the coexistence curves. We reach the cloud curve where—by definition—$\rho_{[0]}=\rho_{[0]}^{\mathrm{c}}$ and determine the density of the coexisting phase on the shadow curve, $\rho_{[0]}^{\mathrm{s}}$. We then choose

$$\rho_{[1]}=\tfrac{1}{2}(\rho_{[0]}^{\mathrm{s}}+\rho_{[0]}^{\mathrm{c}}) \tag{54}$$

and repeat this iteration until we reach $\rho_{\mathrm{cr}}=\lim_{i\to\infty}\rho_{[i]}$ where obviously $\rho_{\mathrm{cr}}=\rho_{[\infty]}^{c}=\rho_{[\infty]}^{s}$.

For reference we have added the phase coexistence curve for a one-component system (“oc”), treated as well in the MSA, characterized by a diameter $\sigma_{\mathrm{oc}}=\sigma_0$ and an amplitude $Z_{\mathrm{oc}}=Z_0$; for this system we extract (via extrapolation) the critical point to be located at $T_{\mathrm{cr;oc}}^*=1.2373$ and $\rho_{\mathrm{cr;oc}}^*=0.32$.

TABLE I. Specification of selected pairs of points (index “1”—low density, index “2”—high density) chosen in the phase diagram of our polydisperse fluid mixture shown in Fig. 1.

Point	Localized on	T^*
A_1,A_2	Binodal curve ($\rho_0=0.03$)	0.9
B_1,B_2	Binodal curve ($\rho_0=0.5$)	0.9
C_1,C_2	Critical binodal ($\rho_{\mathrm{cr}}=0.3523$)	0.9
D_1,D_2	Binodal curve ($\rho_0=0.5$) and intersection with cloud and shadow curve	1.222
E_1,E_2	Cloud and shadow curve	0.9

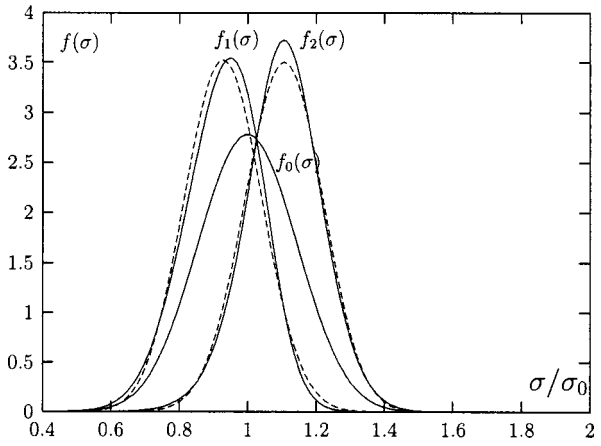

FIG. 2. Mother $[f_0(\sigma)]$ and daughter $[f_1(\sigma)$ and $f_2(\sigma)]$ distribution functions (full curves) for the polydisperse HSY mixture investigated for points A_1 and A_2. Broken curves $-f_1^{\text{beta}}(\sigma)$ and $f_2^{\text{beta}}(\sigma)$ as defined in the text.

On the cloud and on the shadow curve and on the binodals in Fig. 1 we have chosen five pairs of points, labeled by A_i to E_i, $i=1,2$; $i=1$ marks the low-density, gas state point, while $i=2$ indicates the coexisting high-density, liquid state point. Their location in the (T^*,ρ^*) plane is specified in Table I.

A. Phase diagram

We find cloud curves and binodals which are in shape similar to the ones found in the recent van der Waals study.[7] The high density branch of the shadow curve shows however—as the temperature decreases—a behavior different with respect to the van der Waals picture; this will be discussed in the following. Here one should bear in mind that points on the shadow curve represent state points which—at an infinite amount of the incipient phase—coexist with the mother phase. Thus this curve represents a projection of a curve with variable composition in higher dimensional space on the dilution line for which the composition is fixed (see Figs. 2 and 3 in Ref. 2 for a very nice and instructive presentation). The two branches of the binodals for the two selected ρ_0 values terminate on the cloud and the shadow curve. Note that the ρ values for the end points of the respective binodals on the cloud curve are by definition the ρ_0 values of the binodals. Finally we also show the critical binodal, characterized by ρ_{cr}^*, where—by definition—the two end points on the cloud and on the shadow curve merge in one point, the critical point.

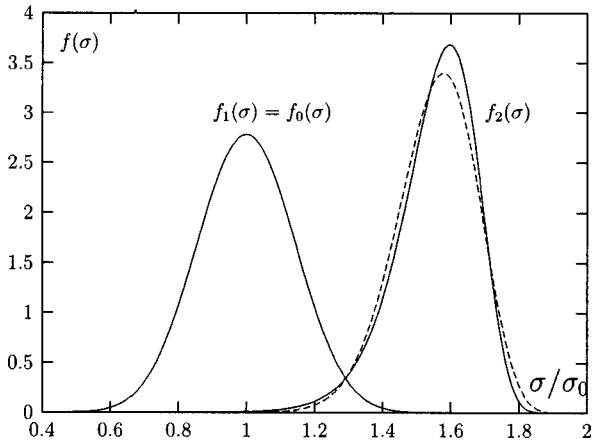

FIG. 4. As in Fig. 2 for points E_1 and E_2.

B. Distribution functions

More specific information about the composition of the coexisting phases can be extracted from the distribution functions of the two daughter phases, which give evidence of possible fractionation effects. For the five selected pairs of points marked in phase diagram, the daughter distribution functions, $f_1(\sigma)$ and $f_2(\sigma)$, along with the mother distribution function, $f_0(\sigma)$, are shown in Figs. 2–6. Points A_i and B_i with $i=1,2$ are general points on the two binodals, characterized by $\rho^*=0.03$ and $\rho^*=0.5$, at a temperature $T^*=0.9$: we observe a moderate fractionation effect and—as expected—a preference for the larger particles for the fluid phase. Points E_1 and E_2 are localized on the cloud and and on the shadow curve at $T^*=0.9$: by definition $f_1(\sigma)=f_0(\sigma)$ and we find a remarkable shift of the maximum of $f_2(\sigma)$ toward larger particles. Points C_1 and C_2 are localized on the critical binodal $(\rho^*=\rho_{\text{cr}}^*)$ at $T^*=0.9$: while the particles of the fluid phase have—on average—nearly the same

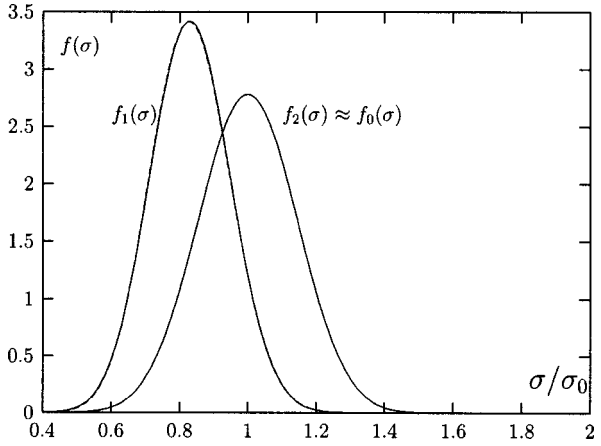

FIG. 3. As in Fig. 2 for points B_1 and B_2.

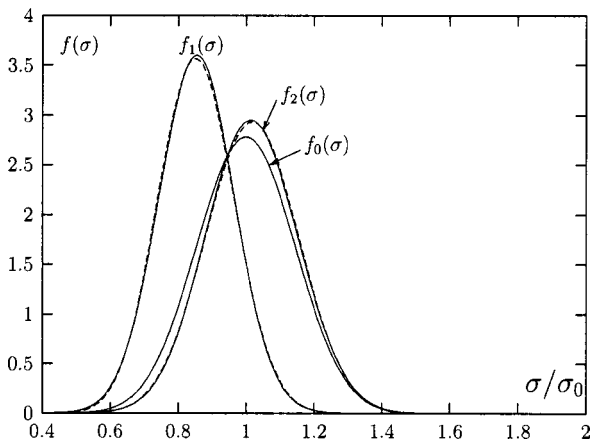

FIG. 5. As in Fig. 2 for points C_1 and C_2.

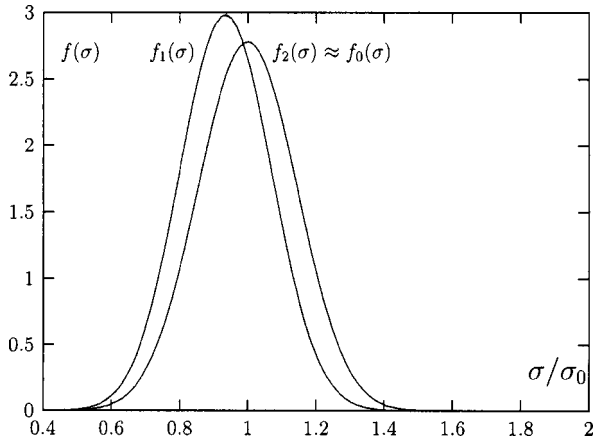

FIG. 6. As in Fig. 2 for points D_1 and D_2.

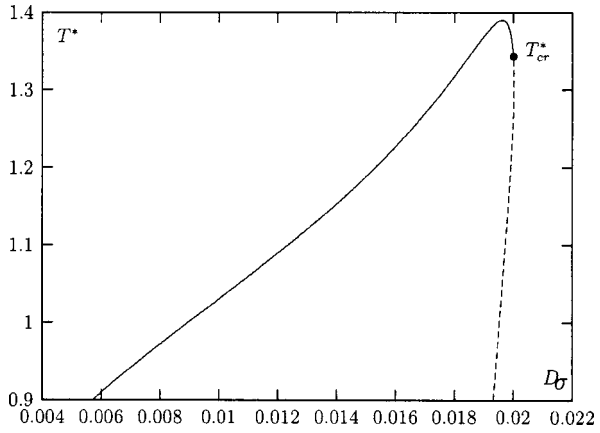

FIG. 8. $D_{\sigma;i}$, $i=1,2$, as defined in Eq. (56) along the shadow curve for the polydisperse HSY mixture investigated in this study. Broken line—gas phase ($i=1$), full line—liquid phase ($i=2$).

size as in the homogeneous mother phase, the particles in the gas phase are on average slightly smaller. Finally we have considered the intersection points of the ($\rho^*=0.5$) binodal with the cloud and the shadow curve (points D_1 and D_2): only a small shift in the mean values of the particle size in the gas phase is observed.

To conclude we have analyzed the *shape* of the daughter distributions functions $f_i(\sigma)$, $i=1,2$, on a more quantitative level: we can thus answer the question if the daughter distribution functions have the same functional shape as the mother distribution function and give a more detailed account on fractionation effects. To be more specific we have investigated how closely the daughter distribution functions $f_i(\sigma)$, $i=1,2$, resemble beta distributions. To this end we have proceeded as follows: from $f_1(\sigma)$ and $f_2(\sigma)$ (determined as described in the previous section), we have calculated the first two moments,

$$\langle \sigma^n \rangle_i = \int_0^\infty d\sigma\, f_i(\sigma)\sigma^n, \quad n=1,2, \quad i=1,2, \tag{55}$$

$$D_{\sigma;i} = \frac{\langle \sigma^2 \rangle_i}{\sigma_0^2} - 1, \quad i=1,2. \tag{56}$$

From these we have determined via Eqs. (35) and (36) beta-distribution functions, $f_i^{\text{beta}}(\sigma)$, for the two daughter phases which are in this sense ''closest'' to the $f_i(\sigma)$; they are shown in Figs. 2–6 in a direct comparison with the $f_i(\sigma)$. We observe that for nearly all selected points considered, the daughter distributions are reasonably well approximated by beta distributions again. Only for points A_i and E_i, $i=1$, 2, larger differences (including a slight shift in the position of the maxima) are observed.

The parameters $\langle \sigma \rangle_i$ and $D_{\sigma;i}$, $i=1,2$, which we have extracted from the numerically determined daughter distribution functions, help us to get a more quantitative insight into possible fractionation effects. We have plotted these quantities along the shadow curve in Figs. 7 and 8 (on the cloud curve these quantities are by definition equal to the corresponding values of the mother distribution) and along the three binodals investigated in this study in Figs. 9 and 10. As the temperature decreases we observe on the shadow curve a strong increase in the mean size of the particles in the fluid phase and a small decrease in the mean size for the particles of the gas phase. From the $D_{\sigma;i}$ curves we learn that the

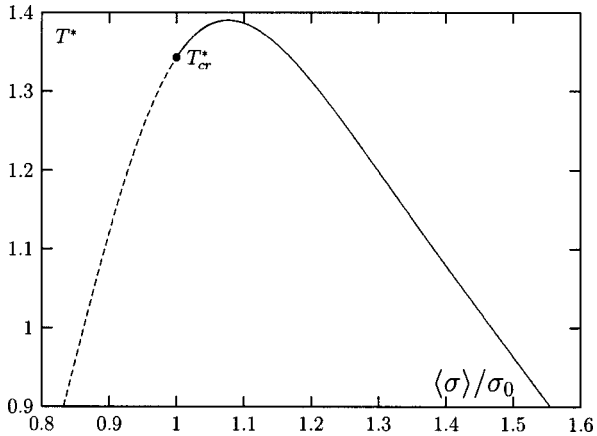

FIG. 7. $\langle \sigma \rangle_i$, $i=1,2$, as defined in Eq. (55) along the shadow curve for the polydisperse HSY mixture investigated in this study. Broken line—gas phase ($i=1$), full line—liquid phase ($i=2$).

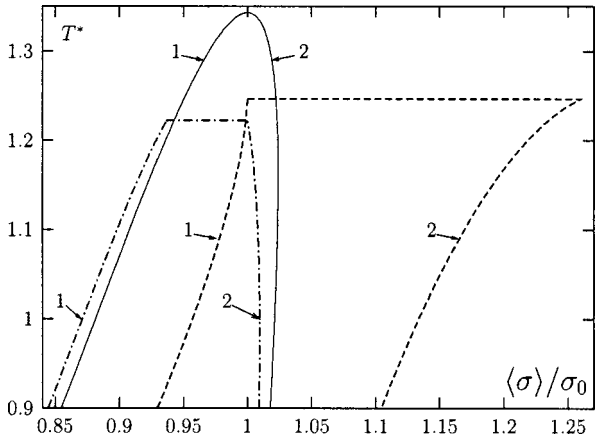

FIG. 9. $\langle \sigma \rangle_i$, $i=1,2$, as defined in Eq. (55) along three binodals for the poly-disperse HSY mixture with the mother phase densities $\rho_0^*=\rho_{cr}^*=0.3527$ (full line), $\rho_0^*=0.03$ (broken line), and $\rho_0^*=0.5$ (dot–dashed line). Here 1 denotes the gas phase and 2 denotes the liquid phase.

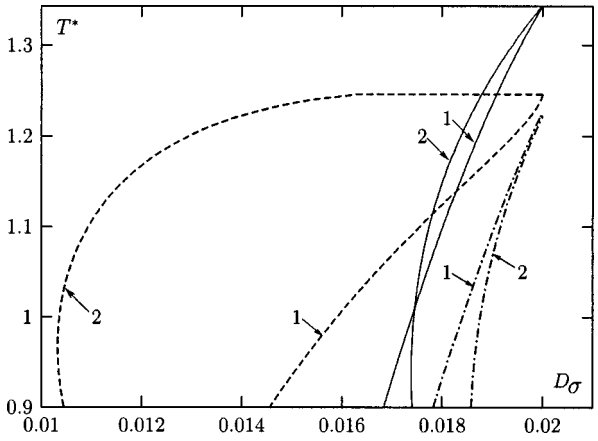

FIG. 10. As in Fig. 9 for $D_{\sigma;i}\,(i=1,2)$ defined by Eq. (56).

width of both daughter distribution functions is smaller than the mother distribution functions: we observe a strong sharpening of the liquid distribution function with decreasing temperature, while the width of the gas phase distribution function remains close to the width of the mother distribution function. We interpret this as follows: the rapid increase in the average size of the particles in the fluid phase due to the temperature decrease (Fig. 7) causes an increase in the overall packing fraction of the liquid shadow phase; in addition, due to the relation between the amplitude of the particles and their size, cf. Eq. (33), lowering the temperature leads to an increase in the strength of interparticle interaction. In an effort to simultaneously maintain the equilibrium with the cloud phase the system responds with a decrease in the density of the shadow phase. This explains the shape of the shadow curve in Fig. 1, where the density of the liquid branch of this curve decreases with decreasing temperature.

For the three binodals considered in this study we find the following for the $\langle\sigma\rangle_i$ curves: again, the average size of the particles in the gas phase is smaller than σ_0. As we can see from Fig. 9, the critical binodal separates two regimes: for $\rho^*<\rho^*_{\mathrm{cr}}$, the mean particle size in the gas phase can reach the value of σ_0 at the temperature where the binodal ends at the cloud curve, while for $\rho^*>\rho^*_{\mathrm{cr}}$, the maximum mean value of the gas phase remains always remarkably smaller than σ_0. This holds—with interchanged roles—for the liquid phase: for $\rho^*>\rho^*_{\mathrm{cr}}$, the mean value of the particles in the liquid phase is close to σ_0, while for densities smaller than the critical density $\langle\sigma\rangle_2$ can reach values that are considerably higher than σ_0. For $D_{\sigma;i}$ the situation is less clear; however we can observe that for a large range of temperatures, the widths of both daughter distributions for densities smaller than the critical density are considerably smaller than D_σ, while for $\rho^*>\rho^*_{\mathrm{cr}}$ we observe only a small narrowing of the $f_i(\sigma)$, $i=1,2$. A more detailed and systematic investigation of these effects will be postponed to a future contribution.

IV. CONCLUSIONS

Solving the MSA for a polydisperse mixture of HSY fluids with factorizable interactions we could show that the system belongs to the class of "truncatable free energy" models; this means that thermodynamic functions required to calculate phase equilibria can be expressed by a finite number of generalized moments. As a consequence we could map the coexistence relations that are particularly complex for polydisperse systems onto a coupled set of highly nonlinear equations for the unknown moments of the daughter distribution functions. We have presented the formalism that leads to these relations along with the relevant expressions for the thermodynamic quantities. Solution of the set of coupled equations for two coexisting phases and for a specific polydisperse mixture leads us to the phase diagram in terms of the cloud and the shadow curve, the critical binodal and binodals for two selected density values. Further we have determined explicitly the daughter distribution functions of the two coexisting phases for five selected pairs of points in the phase diagram and have analyzed them in terms of their functional dependence on the mother distribution. Looking at the first two moments of the daughter distribution functions along the shadow curve and along three binodals we could make quantitative conclusions on fractionation effects induced by the phase transition.

ACKNOWLEDGMENTS

This work was supported by the Österreichischer Forschungsfonds under Project Nos. P14371-TPH and P15785-TPH and by the Österreichische Bundes ministerium für Bildung, Wissenschaft und Kultur under Proj. No. GZ 45.492/1-VI/B/7a/2002. Y.V.K. gratefully acknowledges the hospitality at the CMS and the Institut für Theoretische Physik at the TU Wien where part of this work was performed.

[1] J.-P. Hansen and I. R. McDonald, *Theory of Simple Liquids*, 2nd ed. (Academic, New York, 1986); C. Caccamo, Phys. Rep. **274**, 1 (1996).
[2] P. Sollich, J. Phys.: Condens. Matter **14**, R79 (2002).
[3] B. d'Aguanno and R. Klein, Phys. Rev. A **46**, 7652 (1992).
[4] S. Leroch, G. Kahl, and F. Lado, Phys. Rev. E **59**, 6937 (1999).
[5] S. Leroch, Ph.D. thesis, Technische Universität Wien, 2002.
[6] J. A. Gualteri, J. M. Kincaid, and G. Morrison, J. Chem. Phys. **77**, 52 (1982).
[7] L. Bellier-Castella, H. Xu, and M. Baus, J. Chem. Phys. **113**, 8337 (2000).
[8] L. Blum and J. S. Høye, J. Stat. Phys. **19**, 317 (1978).
[9] E. Arrieta, C. Jędrzejek, and K. N. Marsh, J. Chem. Phys. **95**, 6806 (1991).
[10] M. Ginoza, J. Phys. Soc. Jpn. **55**, 96 (1986).
[11] M. Ginoza and M. Yasutomi, Mol. Phys. **95**, 163 (1998).
[12] J. N. Herrera, L. Blum, and E. Garcia-Llanos, J. Chem. Phys. **105**, 9288 (1996); D. Yurdabak, Z. Akdeniz, and M. P. Tosi, Nuovo Cimento D **16**, 307 (1994).
[13] G. A. Mansoori, N. F. Carnahan, K. E. Starling, and T. W. Leland, J. Chem. Phys. **54**, 1523 (1971).
[14] L. Blum, J. Chem. Phys. **117**, 756 (2002).
[15] J. J. Salacuse and G. Stell, J. Chem. Phys. **77**, 3714 (1982).
[16] M. Abramowitz and I. A. Stegun, *Handbook of Mathematical Functions*, Applied Mathematical Series, Vol. 55 (National Bureau of Standards, Washington, DC, 1964).
[17] G. V. Schultz, Z. Phys. Chem. Abt. B **43**, 25 (1939).
[18] L. Bellier-Castella, M. Baus, and H. Xu, J. Chem. Phys. **115**, 3381 (2001).
[19] C. Tutschka and G. Kahl, Phys. Rev. E **65**, 51104 (2002).